www.czasopisma.pan.pl PAN www.journals.pan.pl
Chemical and Process Engineering 2020, 41 (2), 81–93
DOI: 10.24425/cpe.2019.130225

Principles of modelling of slinky-coil ground heat exchangers

Barbara Larwa*, Krzysztof Kupiec

Cracow University of Technology, Faculty of Chemical Engineering and Technology,
Warszawska St. 24, 31-155 Krakow

The paper presents analytical relationships based on the theory of Green's functions. The relationships refer to instantaneous and continuous as well as point and ring heat sources which are discussed. The relationship relating to continuous ring source is the basis for modelling and designing of spiral ground heat exchangers. Heat transfer in the infinite and semi-infinite body was considered. In the latter case, the image method was discussed. Using the results of measurements regarding heat transfer in the ground with a heat exchanger in the form of a single coil installed, a comparison of calculated ground temperatures with measured values was presented.

Keywords: slinky-coil ground heat exchangers, analytical model of heat transfer

1. INTRODUCTION

Ground source heat pumps are one of the most frequently used devices for heating and cooling buildings, using renewable energy sources. Ground heat exchangers (GHXs) are situated in vertical or horizontal systems. Horizontal systems are characterised by lower investment costs, but they occupy larger land space than systems with vertical probes. With limited ground surface area, it is expedient to use such constructions of horizontal heat exchangers, which are characterised by high packing density of pipes.

In horizontal exchangers, pipes can be installed in a linear, meandering or spiral manner. Slinky heat exchangers are common among the latter (Fig. 1a). The main advantage of these exchangers is that they require less land space than conventional straight horizontal ground heat exchangers. Exchangers of this type are usually placed at a depth of 0.9 m to 1.8 m. Among many kinds of horizontal GHXs, slinky type GHX shows higher thermal efficiency (Yoon et al., 2015).

The first information about slinky-coil ground heat exchangers was presented by Bose and Smith (1992). Studies of ground exchangers with slinky coils concentrate on modelling using numerical applications, analytical solutions and experimental research. Recently, analytical solutions are often used in the studies of slinky-coil exchangers: Cui et al. (2011), Jeon et al. (2018) and Kim et al. (2018), Li et al. (2012), Wang et al. (2016), Xiong et al. (2015), Zhang et al. (2015). Analytical solutions of spiral exchanger models are based on the Green's function theory and the method of images (Carslaw and Jaeger, 1959).

The model formulated by Xiong et al. (2015) relies on analytical ring source solutions to compute temperature response functions for slinky-coil heat exchangers. The thermal effect of the ground surface

* Corresponding author, e-mail: barbara.larwa@pk.edu.pl

temperature variation on the GHXs is considered by superimposing the undisturbed ground temperature, which is calculated using the numerical approach. Li et al. (2012) proposed a moving ring source model considering the influence of subsoil water flow to study the temperature response of the horizontal slinky-coil GHX and multiple performance.

Sangi and Muller (2018) developed a Modelica-model for the slinky-coil horizontal GHX. The heat transfer model between the working fluid and pipe wall was developed by the Modelica Standard Library (MSL). Kim et al. (2018) established a 3D numerical model of horizontal GHX with CFD software. Go et al. (2016) established a three-dimensional model of a horizontal spiral-coil loop to investigate thermal behaviour. A numerical analysis was performed with the commercial program COMSOL Multiphysics, which is a computer code based on the finite element method (FEM), coupled with computational fluid dynamics (CFD) analysis.

The purpose of this work was to present the basics of modelling ground spiral exchangers. Analytical dependencies and their graphic interpretations are presented. Using the results of measurements presented in the literature, calculated ground temperatures were compared with measured values. The presented considerations and research results relate to one ring of an exchanger.

2. ASSUMPTIONS USED IN MATHEMATICAL MODELS

A pipe system used in slinky heat exchangers is shown in Fig. 1a. In matters related to modelling heat transfer in such a system, several simplifying assumptions should be made. The most important of them are presented below.

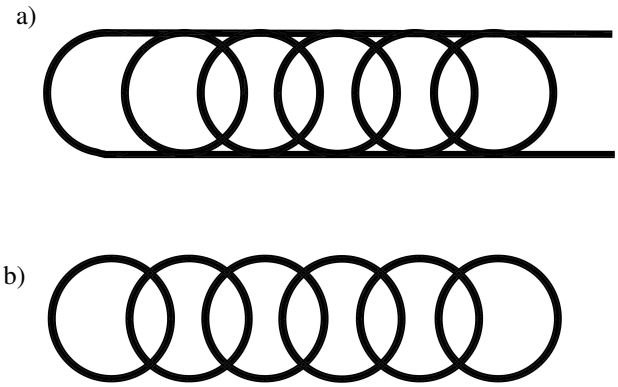

Fig. 1. Slinky-coil ground heat exchanger: a) real system b) model system

a) In the ring source model, the configuration of slinky exchanger pipes is simplified to a ring arrangement, as shown in Fig. 1b.
b) It is assumed that the rate of heat transfer for each ring is the same and the heat flux over the entire circumference of the ring is uniform.
c) The ground is treated as a homogeneous semi-infinite body; the ground's thermal properties do not change with both location and time.
d) Changes in the ground temperature with the exchanger installed result from the superposition of two independent elementary processes:
   - heat transfer caused by heat sources at a constant ground surface temperature,
   - heat transfer caused by the ground surface temperature changing over time.

The equation of heat conduction in a three-dimensional space, with the presence of internal heat sources, has the form:

$$\frac{\partial \vartheta}{\partial t} = \alpha \left(\frac{\partial^2 \vartheta}{\partial x^2} + \frac{\partial^2 \vartheta}{\partial y^2} + \frac{\partial^2 \vartheta}{\partial z^2} \right) + \frac{q_v}{c_v} \tag{1}$$

where q_v is the rate of heat generation.

According to assumption d), the temperature at any point of the ground is the sum of the temperature T_0 resulting from changes in the surface temperature of the ground and the temperature excess (temperature responses) ϑ resulting from the operation of heat sources:

$$T = T_0 + \vartheta \tag{2}$$

In the general case, the temperature T_0 is variable over time, which results from changing environmental conditions.

3. SINGLE RING IN AN INFINITE MEDIUM

It is assumed that the ground is characterised by thermal diffusivity α and volumetric heat capacity c_v. In the initial state, the ground temperature excess is zero.

Considering the organization of time, the heat source may be instantaneous or continuous. In addition, heat sources have different geometric shapes. The individual combinations of instantaneous and continuous sources as well as point and ring sources are considered below. The simplest form of a ring-shaped exchanger is a single ring placed deep in the ground (infinite medium).

3.1. Instantaneous point source

The basic relationship concerns the distribution of heat in an infinite medium from an instantaneous point source. If at time $t = 0$ heat is released at a certain point in space in the amount of Q, then at point P distant by d from the source, the temperature excess after time t is (Carslaw and Jaeger, 1959):

$$\vartheta = \frac{Q}{8c_v \left(\pi \alpha t\right)^{3/2}} \cdot \exp\left(-\frac{d^2}{4\alpha t}\right) \tag{3}$$

Temporal courses of the ground temperature excess, in the form of lines, for instantaneous source at a point distant from the source by $d = 0.2$ m, are presented in Fig. 2. Various values of heat Q released at $t = 0$ were adopted: 0.8 MJ, 2.0 MJ and 4.0 MJ. Calculations were carried out for $\alpha = 0.60 \times 10^{-6}$ m^2/s and $c_v = 2.0 \times 10^6$ J/(m^{3}K). Initially, the value of ϑ increased suddenly, reached a maximum, and then decreased with time reaching zero. The maximum value of the temperature excess is proportional to the amount of heat released.

3.2. Continuous point source

If the source generates heat continuously, the temperature excess is the sum of the excesses in individual time intervals. For a constant power $\dot{Q}$ of a point source, the excess temperature at a point distant from the source by d after time t can be calculated by integrating Eq. (3) with respect to time (Appendix A). The dependence on the temperature excess has the form:

$$\vartheta = \frac{\dot{Q}}{4\pi k d} \cdot \operatorname{erfc}\left(\frac{d}{2\sqrt{\alpha t}}\right) \tag{4}$$

In Fig. 2 temporal courses of the ground temperature excess, in the form of symbols, for continuous source at a point distant from the source by $d = 0.2$ m, are depicted. Different values of thermal power of the continuous source $\dot{Q}$ were adopted: 4 W, 10 W and 20 W ($\alpha = 0.60\times10^{-6}$ m^2/s and $c_v = 2.0\times10^6$ J/(m^{3}K)). For a continuous source, a permanent increase in temperature excess was observed, with the ϑ value being proportional to the thermal power of the source.

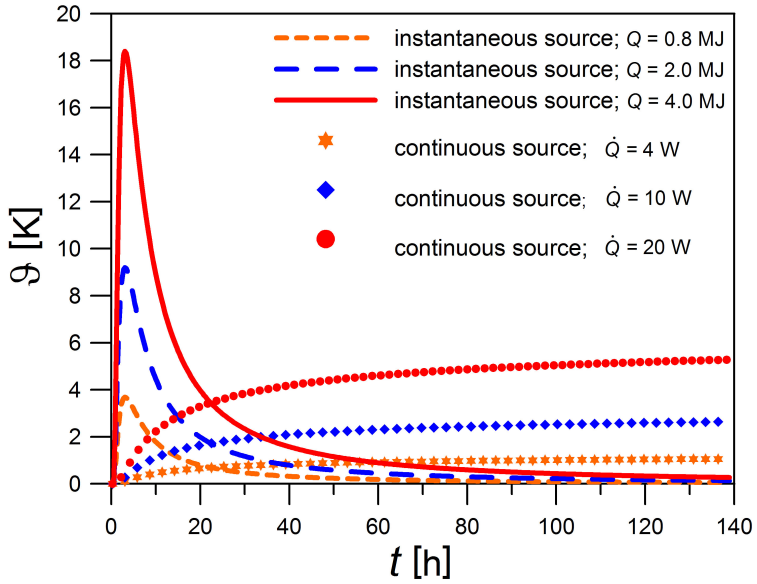

Fig. 2. Courses of the temperature excesses for point sources: instantaneous and continuous

3.3. Instantaneous ring source

Point sources located on a circle with radius R form a ring source. In Fig. 3 a ring-shaped source and any P point in space in two projections, were depicted. Point B is a projection of point P on the plane on which the source lies ($y - x$). The distance from point P to the heat source A is denoted as d. The position of point A on the circle is determined by the rotation angle σ. The relationship between distance d and angle σ should be determined. The geometry of the system, shown in Fig. 3a, indicates that:

$$\overline{AB}^2 = \overline{AC}^2 + \overline{CB}^2 = (R\sin\sigma)^2 + (r - R\cos\sigma)^2 \tag{5}$$

while, in Fig. 3b a following relationship is demonstrated:

$$d^2 = \overline{AB}^2 + z'^2 \tag{6}$$

Therefore, the dependency sought has the form:

$$d = \sqrt{(R\sin\sigma)^2 + (r - R\cos\sigma)^2 + z'^2} = \sqrt{r^2 + R^2 + z'^2 - 2rR\cos\sigma} \tag{7}$$

The relationship for the instantaneous point source (3) should be integrated with respect to the angle σ in the range from 0 to π. The relationship is as follows (Carslaw and Jaeger, 1959):

$$\vartheta = \frac{Q}{8c_v\,(\pi\alpha t)^{3/2}} \cdot \exp\left(-\frac{r^2 + R^2 + z'^2}{4\alpha t}\right) \cdot I_0\left(\frac{rR}{2\alpha t}\right) \tag{8}$$

where I_0 is the modified Bessel function of the first kind of order zero. Derivation of Equation (8) is presented in Appendix B.

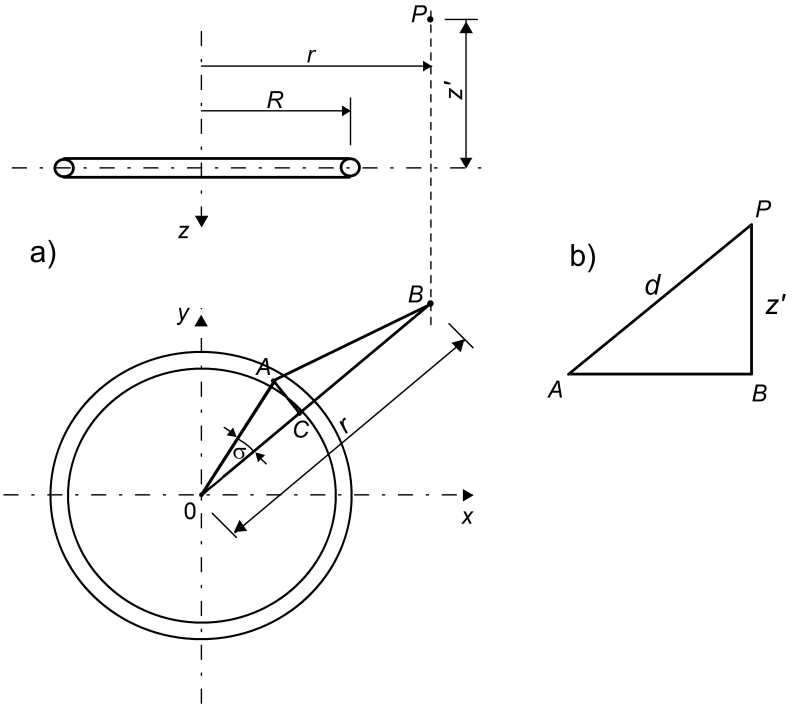

Fig. 3. Ring heat source

In Fig. 4 graphical interpretation of Eq. (8) in the form of temperature profiles at various process times is shown. The graph applies to the following process parameter values: $z' = 0.2$ m, $R = 0.5$ m, $\alpha = 0.60\times10^{-6}$ m^2/s, $c_v = 2.0 \times 10^6$ J/(m^{3}K) and $Q = 2$ MJ. For short process duration, temperature excesses reach the highest values for $x = \pm R$ i.e. for the coordinate value corresponding to the location of the heat source. Values of ϑ for short times increase with the passage of time. However, for longer times, the temperature profiles flatten, and the values of temperature excesses decrease over time, reaching zero.

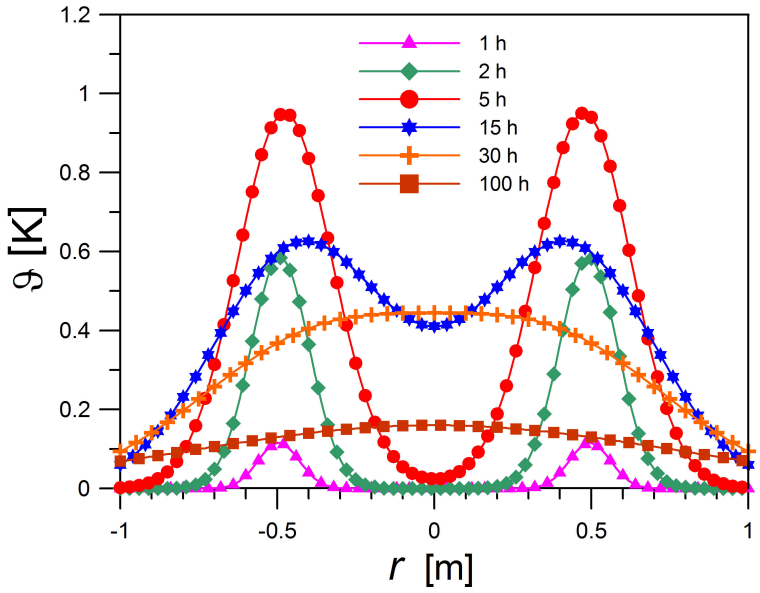

Fig. 4. Temperature profiles around ring-shaped instantaneous heat source

3.4. Continuous ring source

When designing or modelling slinky-coil ground heat exchangers, the most important is the case of a continuous ring source. The relationship to determine temperature excesses in this case can be derived from Eqs. (4) or (8).

Eq. (4) applies to a continuous point source. By integrating this relationship to the angle σ (Fig. 3) in the range from 0 to 2π a relationship for a continuous ring source is obtained (Li et al., 2012):

$$\vartheta = \frac{\dot{Q}}{8\pi^2 k} \int_0^{2\pi} \frac{1}{d} \operatorname{erfc}\left(\frac{d}{2\sqrt{\alpha t}}\right) d\sigma \tag{9}$$

The integral value should be determined numerically. From Eq. (9) the temperature in the heat source itself cannot be calculated (for $d = 0$ applies $\vartheta \to \infty$).

The relationship for a continuous ring source can also be derived from Eq. (8) by integration over time in the range from 0 to t. Therefore, Eq. (10) is obtained (Xiong et al., 2015):

$$\vartheta = \frac{1}{8c_v\,(\pi\alpha)^{3/2}} \int_0^t \frac{\dot{Q}}{\tau^{2/3}} \cdot \exp\left(-\frac{r^2 + R^2 + z'^2}{4\alpha\tau}\right) \cdot I_0\left(\frac{rR}{2\alpha\tau}\right) d\tau \tag{10}$$

In Fig. 5 dependences of temperature excesses on the location in the vicinity of a ring-shaped continuous heat source are presented. The following process parameter values were adopted: $R = 0.5$ m, $\alpha = 0.60 \times 10^{-6}$ m^2/s, $c_v = 2.0 \times 10^6$ J/(m^{3}K), $\dot{Q} = 400$ W and $t = 100$ h. For calculations Eqs. (9) or (10) were used. Due to the symmetry of the system, only the part of the graph regarding positive r values is presented. The compatibility of the ϑ values obtained according to both relationships is very good. Discrepancies occur only close to $r = \pm R$ and $z' = 0$, i.e. in places where the heat sources are located. It results from the fact that according to Eq. (9) for these variable position values the function is discontinuous and reaches values $\vartheta \to \infty$.

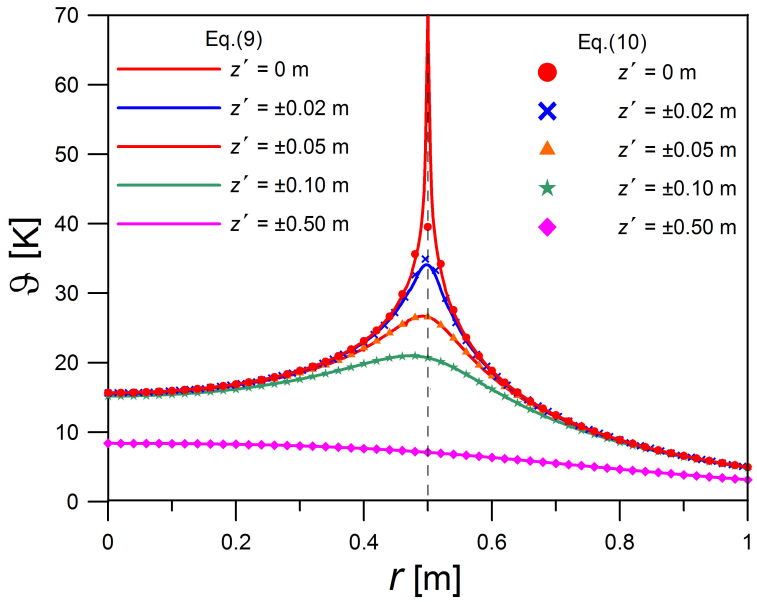

Fig. 5. Temperature profiles for a continuous ring source determined according to Eqs. (9) and (10)

In Fig. 6 a schematic diagram of relationships between dependencies regarding individual heat sources is depicted. The basis of all presented relationships is Eq. (3) regarding the instantaneous point source.

The final Eqs. (9) or (10) for a continuous ring source are obtained by integrating Eq. (3) twice: with respect to time and with respect to the angle determining the position on the circumference of the ring. Depending on the order in which integration is performed, after the first integration Eq. (4) or (8) is obtained.

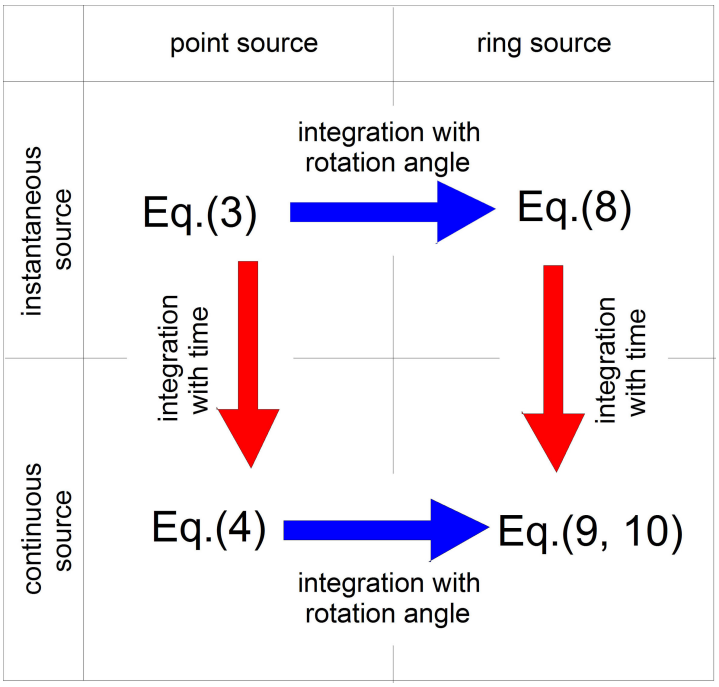

Fig. 6. Relationship between individual dependencies

4. SINGLE RING IN A SEMI-INFINITE MEDIUM

If the distance between the heat source and the ground surface h is small, the ground should be treated as a semi-infinite body. In this case, in the model describing heat transfer, the method of images is used, in which the surface effect is considered via a virtual heat source placed symmetrically with respect to the real source, as shown in Fig. 7. Therefore, the temperature at any point P is influenced by both sources: real and virtual. For a semi-infinite body, it is convenient to use a z coordinate ($z = h - z'$) determining the distance from the ground surface (Fig. 7).

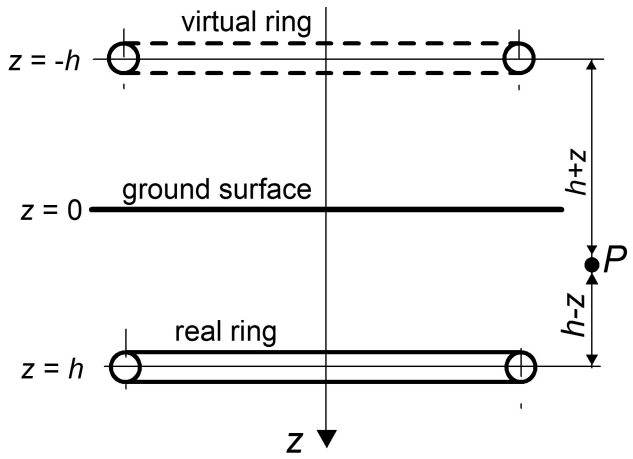

Fig. 7. Image method

If the temperature of the ground surface can be considered unchanged over time, the virtual source is negative (heat sink) and the relationship describing the temperature excess in the semi-infinite body is defined by (Xiong et al., 2015):

$$\vartheta = \frac{1}{8c_v\,(\pi\alpha)^{3/2}} \int_0^t \frac{\dot{Q}}{\tau^{3/2}}\,(E_{real} - E_{virt}) \cdot I_0\left(\frac{rR}{2\alpha\tau}\right) d\tau \tag{11}$$

where E_{real} is the expression in Eq. (10):

$$E_{real} = \exp\left(-\frac{r^2 + R^2 + z'^2}{4\alpha\tau}\right) = \exp\left(-\frac{r^2 + R^2 + (h-z)^2}{4\alpha\tau}\right) \tag{12}$$

Quantity E_{virt}, according to Fig. 7, is defined as follows:

$$E_{virt} = \exp\left(-\frac{r^2 + R^2 + (h+z)^2}{4\alpha\tau}\right) \tag{13}$$

If the surface of a semi-infinite body is impervious to heat, then a virtual heat source is positive and Eq. (11) should be modified to a form, where there is a sum instead of a difference: $E_{real} + E_{virt}$.

A similar procedure for adjusting the form of the equation for a semi-infinite body applies to Eq. (9). For a constant ground surface temperature for the semi-finite body Eq. (14), instead of Eq. (9), applies:

$$\vartheta = \frac{\dot{Q}}{8\pi^2 k} \int_0^{2\pi} \left[\frac{1}{d_{real}}\operatorname{erfc}\left(\frac{d_{real}}{2\sqrt{\alpha t}}\right) - \frac{1}{d_{virt}}\operatorname{erfc}\left(\frac{d_{virt}}{2\sqrt{\alpha t}}\right)\right] d\sigma \tag{14}$$

where distances d_{real} and d_{virt} according to Eq. (7) and Fig. 7 are equal to:

$$d_{real} = \sqrt{(R\sin\sigma)^2 + (r - R\cos\sigma)^2 + (h-z)^2} \tag{15a}$$

$$d_{virt} = \sqrt{(R\sin\sigma)^2 + (r - R\cos\sigma)^2 + (h+z)^2} \tag{15b}$$

The ground temperature profiles for different depths h of installing the heat source, different process durations and different conditions on the ground surface are depicted in Figs 8 a and b. Calculations were carried out for a single ring and the following process parameter values: $R = 0.5$ m, $r = 0$ m, $\alpha = 0.60 \times 10^{-6}$ m^2/s, $c_v = 2.0 \times 10^6$ J/(m^{3}K), $\dot{Q} = 100$ W. For short process durations (1 day), changes in the ground temperature were local and even for small h values (1 m) they did not include the surface of the ground (Fig. 8a). Therefore, the conditions on the ground surface do not affect the temperature profiles.

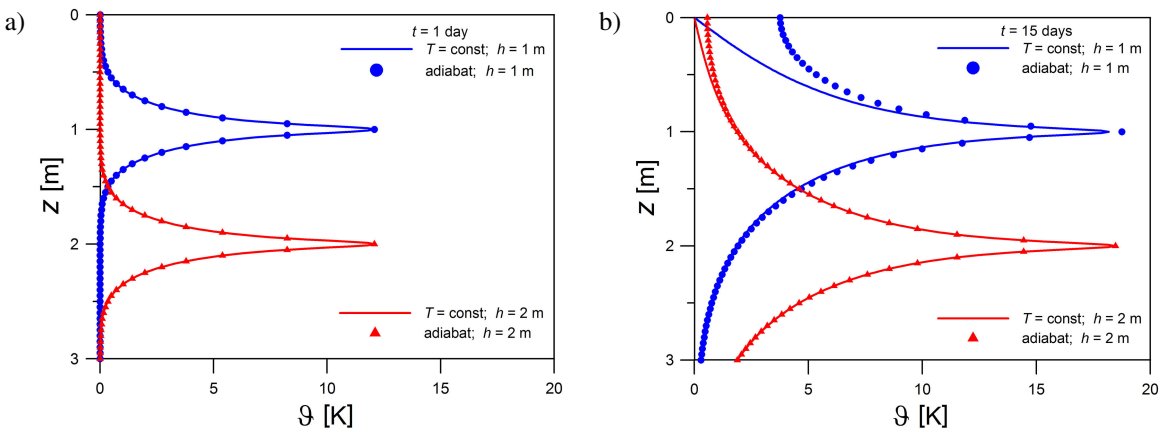

Fig. 8. Ground temperature profiles for different process durations: a) $t = 1$ day; b) $t = 15$ days

For longer process times (15 days), the ground surface conditions are important, especially for a shallow depth of the heat source's location (Fig. 8b). Near the ground surface ($z = 0$), temperature profiles at a constant surface temperature differ significantly from the profiles corresponding to the surface impervious to heat. For a constant temperature of the ground surface, the temperature excesses become zero: $(\vartheta)_{z=0} = 0$, whereas when the ground surface is impervious to heat, the temperature gradient is zero: $(d\vartheta/dz)_{z=0} = 0$ that is, the temperature profile lines become vertical.

5. EXPERIMENTAL VERIFICATION

The verification of the analytical relationships presented above was carried out by comparing the results of calculations with the results of experimental tests presented by Larwa et al. (2019). The research concerned one coil of a spiral exchanger placed in the ground at a depth of 0.5 m. A coil with a diameter of 1 m was a polyethylene pipe with transverse dimensions of 32/26 mm. The exchanger was fed with water at a temperature of 54.5 °C flowing with a flow rate of 0.104 m^3/s. The duration of the experiment was 3 days. Temperature of the ground at various depths was measured. The water temperature at the outlet of the exchanger was also monitored. A scheme of the experimental set-up is shown in Fig. 9.

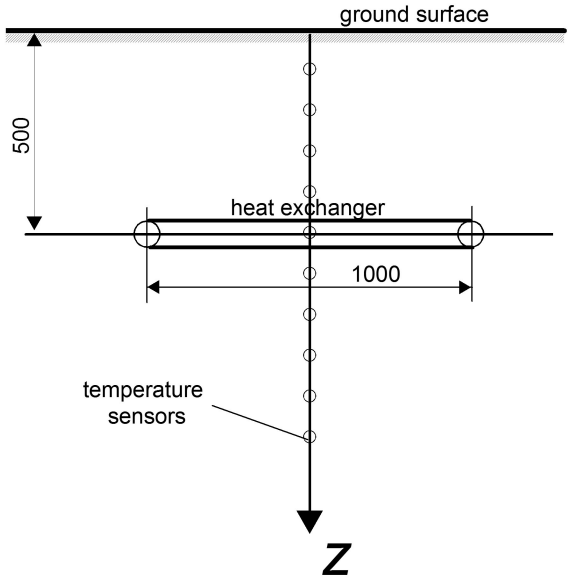

Fig. 9. Scheme of the measuring system

Due to the temporal increase in the ground temperature, the water temperature at the outlet from the heat exchanger increased, and the thermal power transferred to the ground decreased over time. Based on the results of water temperature measurements, the relationship between the rate of heat transfer and the duration of the process was approximated by (Larwa et al., 2019):

$$\dot{Q} = 410 + 221 \cdot \exp(-0.57 \cdot 10^{-3} \cdot t) \tag{16}$$

For the conditions under which the tests were conducted, the calculated values of the ground temperature in the ring axis ($r = 0$) at various depths were determined. The ground's thermal properties were: $\alpha = 0.841 \times 10^{-6}$ m^2/s, $c_v = 2.94 \times 10^6$ $J/(m^3K)$ (Larwa et al., 2019). Due to the temporal variability of $\dot{Q}$, Eq. (11) was used in the calculations. The value of the integral was determined numerically using the Simpson method.

The determined temperature excesses were converted into the ground temperature according to Eq. (2). The fact that if the relatively short duration of the process (in relation to the length of the heating season) was considered, then the daily averaged ground surface temperature could be treated as unchanged in time, and the temperature T_0 – treated as the initial temperature T_{init}. Experimentally determined initial ground temperature profile has the form $T_{init} = 5.23z - 0.14$.

A comparison of experimental and computational results for various process times is given in Fig. 10. The graph shows the ground temperature profiles in the ring axis ($r = 0$). Calculations as well as experiments show that the temperature on the ground surface was constant over time and amounted to 0 °C. In addition, as expected, the ground temperature reached its maximum at the depth of the exchanger ($z = 0.5$ m). The agreement between experimental and computational results is satisfactory.

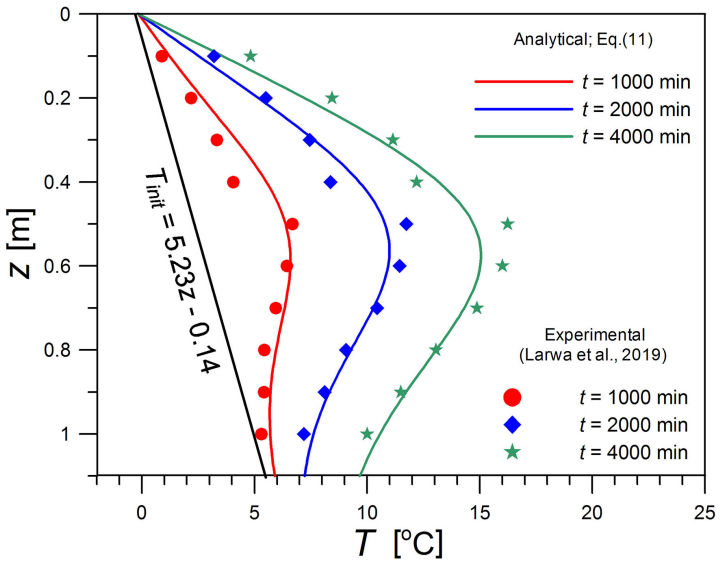

Fig. 10. Comparison of experimental and analytical results according to Eq. (11)

6. CONCLUSIONS

- A comparison of ground temperature values determined based on analytical dependence (11) with the values determined experimentally and presented in the work by Larwa et al. (2019) confirms the validity of using analytical dependencies based on Green's functions theory for modelling heat transfer in spiral ground heat exchangers.
- The lack of symmetry of temperature profiles, relative to the plane on which the heat exchanger was located ($z = 0.5$ m), results from the heterogeneous initial soil temperature profile and the impact of the environment.
- Compliance of analytical results and experimental values for a single ring is the basis for modelling multiple ring systems.

SYMBOLS

c_v volumetric heat capacity of the ground, J/(m^{3}K)
d distance of the P point from the heat source, m
h distance between the heat source and the ground surface, m
k thermal conductivity of the ground, W/(mK)

q_v rate of heat generation per unit of volume, W/m^3
Q amount of heat, J
$\dot{Q}$ rate of heat transfer (power of heat source) per one ring, W
r distance from the axis of the ring source, m
R radius of ring, m
t time, s
T temperature, °C
x, y, z position coordinates, m
z' distance from the plane of the ring source, m

Greek symbols

α thermal diffusivity of the ground, m^2/s
σ rotation angle, rad
τ integration variable
ϑ temperature excess, K

Subscripts

init initial
real real heat source
virt virtual heat source

REFERENCES

Abramowitz M., Stegun I.A., 1972. *Handbook of mathematical functions with formulas, graphs, and mathematical tables*. 9th edition, New York, 358-364.

Bose J.E., Smith M.D., 1992. Performance of new ground heat exchanger configurations for heat pumps. *Solar Eng.*, 1, 385–393.

Carslaw H.S., Jaeger J.C., 1959. *Conduction of heat in solids*. 2nd edition, Clarendon Press, Oxford.

Cui P., Li X., Man Y., Fang Z., 2011. Heat transfer analysis of pile geothermal heat exchangers with spiral coils. *Appl. Energy*, 88, 4113–4119. DOI: 10.1016/j.apenergy.2011.03.045.

Go G.H., Lee S.R., Yoon S., Kim M.J., 2016. Optimum design of horizontal ground-coupled heat pump systems using spiral-coil-loop heat exchangers. *Appl. Energy*, 162, 330-345. DOI: 10.1016/j.apenergy.2015.10.113.

Jeon J.S., Lee S.R., Kim M.J., 2018. A modified mathematical model for spiral coil type horizontal ground heat exchangers. *Energy*, 152, 732–743. DOI: 10.1016/j.energy.2018.04.007.

Kim M.J., Lee S.R., Yoon S., Jeon J.S., 2018. An applicable design method for horizontal spiral-coil-type ground heat exchangers. *Geothermics*, 72, 338–347. DOI: 10.1016/j.geothermics.2017.12.010.

Larwa B., Teper M., Grzywacz R., Kupiec K., 2019. Study of a slinky-coil ground heat exchanger – Comparison of experimental and analytical solution. *Int. J. Heat Mass Transfer*, 142, 118438. DOI: 10.1016/j.ijheatmasstransfer.2019.118438.

Li H., Nagano K., Lai Y., 2012. A new model and solutions for a spiral heat exchanger and its experimental validation. *Int. J. Heat Mass Transfer*, 55, 4404–4414. DOI: 10.1016/j.ijheatmasstransfer.2012.03.084.

Li H., Nagano K., Lai Y., 2012. Heat transfer of a horizontal spiral heat exchanger under groundwater advection. *Int. J. Heat Mass Transfer*, 55, 6819–6831. DOI: 10.1016/j.ijheatmasstransfer.2012.06.089.

Sangi R., Muller D., 2018. Dynamic modelling and simulation of a slinky-coil horizontal ground heat exchanger using Modelica. *J. Build. Eng.*, 16, 159–168. DOI: 10.1016/j.jobe.2018.01.005.

Wang D., Lu L., Cui P., 2016. A new analytical solution for horizontal geothermal heat exchangers with vertical spiral coils. *Int. J. Heat Mass Transfer*, 100, 111–120. DOI: 10.1016/j.ijheatmasstransfer.2016.04.001.

Wang D., Lu L., Cui P., 2016. A novel composite-medium solution for pile geothermal heat exchangers with spiral coils. *Int. J. Heat Mass Transfer*, 93, 760–769. DOI: 10.1016/j.ijheatmasstransfer.2015.10.055.

Xiong Z., Fisher D.E., Spitler J.D., 2015. Development and validation of a slinky ground heat exchanger model. *Appl. Energy*, 141, 57–69. DOI: 10.1016/j.apenergy.2014.11.058.

Yoon S., Lee S.R., Go G.H., 2015. Evaluation of thermal efficiency in different types of horizontal ground heat exchangers. *Energy Build.*, 105, 100–105. DOI: 10.1016/j.enbuild.2015.07.054.

Zhang W., Yang H., Cui P., Lu L., Diao N., Fang Z., 2015. Study on spiral source models revealing groundwater transfusion effects on pile foundation ground heat exchangers. *Int. J. Heat Mass Transfer*, 84, 119–129. DOI: 10.1016/j.ijheatmasstransfer.2014.12.036.

Received 15 November 2019
Received in revised form 3 April 2020
Accepted 6 April 2020

APPENDIX A

Derivation of relationships for a continuous point source

The dependence on the temperature excess after time t for a continuous point source is obtained by applying in Eq. (3) the substitution $Q = \dot{Q} \cdot d\tau$ and integration in the range from 0 to t.

$$\vartheta = \int_0^t \frac{\dot{Q}}{8c_v\,(\pi\alpha\tau)^{3/2}} \exp\left(-\frac{d^2}{4\alpha\tau}\right) d\tau \tag{A1}$$

where τ is the integration variable. A new variable has been introduced into Eq. (A1):

$$\zeta = \frac{d}{2\sqrt{\alpha\tau}} \tag{A2}$$

The substitution implies that:

$$\tau = \frac{d^2}{4\alpha} \cdot \frac{1}{\zeta^2} \qquad \text{and} \qquad d\tau = -\frac{d^2}{2\alpha} \cdot \frac{1}{\zeta^3} d\zeta \tag{A3a,b}$$

Taking into account the above relationships in Eq. (A1), we obtain:

$$\vartheta = \frac{\dot{Q}}{4\pi c_v \alpha d} \frac{2}{\sqrt{\pi}} \int_\zeta^\infty \exp\left(-\zeta^2\right) d\zeta \tag{A4}$$

Because $\alpha c_v = k$ and

$$\frac{2}{\sqrt{\pi}} \int_\zeta^\infty \exp\left(-\zeta^2\right) d\zeta = \operatorname{erfc}\left(\frac{d}{2\sqrt{\alpha t}}\right) \tag{A5}$$

so

$$\vartheta = \frac{\dot{Q}}{4\pi k d} \operatorname{erfc}\left(\frac{d}{2\sqrt{\alpha t}}\right) \tag{A6}$$

APPENDIX B

Derivation of relationships for an instantaneous ring source

Equation (3) is also the basis for the dependence on the temperature excess for the instantaneous ring source. Determine the average total value of the excess temperature in relation to the angle σ within the range of 0 to π. And so

$$\vartheta = \frac{1}{\pi}\int_0^{\pi} \frac{Q}{8c_v\,(\pi\alpha t)^{3/2}} \cdot \exp\left(-\frac{d^2}{4\alpha t}\right) d\sigma \tag{B1}$$

Taking into consideration Eqs. (B1) and (7) (B2) is obtained

$$\vartheta = \frac{Q}{8c_v\,(\pi\alpha t)^{3/2}}\frac{1}{\pi}\int_0^{\pi} \exp\left(-\frac{r^2 + R^2 + z'^2 - 2rR\cos\sigma}{4\alpha t}\right) d\sigma \tag{B2}$$

and after transformation

$$\vartheta = \frac{Q}{8c_v\,(\pi\alpha t)^{3/2}} \exp\left(-\frac{r^2 + R^2 + z'^2}{4\alpha t}\right) \cdot \frac{1}{\pi}\int_0^{\pi} \exp\left(\frac{rR}{2\alpha t}\cos\sigma\right) d\sigma \tag{B3}$$

The modified Bessel function of the first kind of order zero is defined as follows (Abramowitz and Stegun, 1972; Cui et al., 2011):

$$I_0(x) = \frac{1}{\pi}\int_0^{\pi} \exp(x \cdot \cos\zeta) d\zeta \tag{B4}$$

So

$$\vartheta = \frac{Q}{8c_v\,(\pi\alpha t)^{3/2}} \exp\left(-\frac{r^2 + R^2 + z'^2}{4\alpha t}\right) \cdot I_0\left(\frac{rR}{2\alpha t}\right) \tag{B5}$$